10.1098/rspa.2001.0841

On the dynamics of a vertically driven damped planar pendulum

By M. V. Bartuccelli[1], G. Gentile[2] and K. V. Georgiou[1]

[1]*Department of Mathematics and Statistics, University of Surrey, Guildford GU2 7XH, UK*

[2]*Dipartimento di Mathematica, Università di Roma Tre, Roma I-00146, Italy*

Received 9 August 2000; revised 7 December 2000 and 8 March 2001; accepted 10 April 2001

Results on the dynamics of the planar pendulum with parametric vertical time-periodic forcing are reviewed and extended. Numerical methods are employed to study the various dynamical features of the system about its equilibrium positions. Furthermore, the dynamics of the system far from its equilibrium points is systematically investigated by using phase portraits and Poincaré sections. The attractors and the associated basins of attraction are computed. We also calculate the Lyapunov exponents to show that for some parameter values the dynamics of the pendulum shows sensitivity to initial conditions.

Keywords: basins of attraction; attractors; Poincaré sections; Lyapunov exponents

1. Introduction

Over the past few decades, parametrically excited nonlinear oscillators have begun to be extensively studied, both theoretically and numerically. Their dynamics is generally very complicated even when only one and a half degrees of freedom are involved: this shows that the complex behaviour does not arise from a large number of variables, but from the nonlinearity of the equation of motion.

Below, a planar pendulum whose point of support (pivot) is subjected to vertical sinusoidal displacement is studied. This system has two equilibrium configurations: the downward position and the upward position. It is known that the upward equilibrium state can be made stable by subjecting the pivot to a harmonic vertical oscillation of appropriate frequency and amplitude. Stephenson (1908) was the first to predict theoretically this remarkable result, and the idea has reappeared in a number of subsequent studies (Ness 1967; Kalmus 1970; Koch *et al*. 1983; Koch & Leven 1985; Michaelis 1985; Pippard 1987; Leiber & Risken 1988; Blackburn *et al*. 1992*a*, *b*; Acheson 1993, 1995, 1997; Aceson & Mullin 1993).

Analytically, in the absence of friction, the stability of the upward position is usually obtained by the method of *averaging* (see Kapitsa 1951; Landau & Lifshitz 1976; Percival & Richards 1982), which, however, is not completely satisfactory, as pointed out by Blackburn *et al*. (1992*b*) and Bartuccelli *et al*. (2001*a*). More specifically, Bartuccelli *et al*. (2001*a*) rigorously show that the upward position can become stable by proving the existence of Kolmogorov–Arnold–Moser (KAM) invariant curves arbitrarily close to the equilibrium point: such curves produce a topological obstruction for the trajectories arising from initial data contained in the open bounded

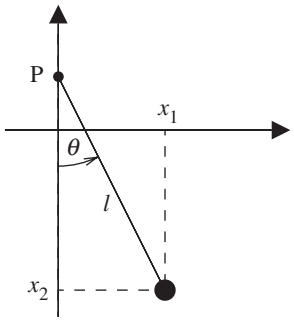

Figure 1. The pendulum with the point of support oscillating on a vertical line.

region internal to them. In Bartuccelli *et al.* (2001*b*), we consider the same situation, but in the presence of (small) friction (as in the present paper), and we prove that the upward equilibrium position of the driven pendulum does indeed become stable if the period of the forcing is small enough, in agreement with both numerical computations and graphic visualization.

In this paper we employ numerical techniques to make detailed studies of such a system in the presence of friction. We shall investigate the stability of both fixed points and study their basins of attraction when they are (asymptotically) stable. We shall also investigate the existence of other attractors, and again determine the corresponding basins of attraction; analogous results for similar models can be found in literature (see Smith & Blackburn 1989, 1992; Blackburn *et al.* 1992*a*, *b*; Capecchi & Bishop 1994). Furthermore, we also find strong numerical evidence that the union of the basins of attraction fills the entire phase space: in other words *any* initial condition will eventually end up on one of the attractors. As far as we know, such a result has not appeared in the literature so far.

Numerical Poincaré sections (see Poincaré 1899; Henon 1982; Hilborn 1994) and phase portraits (see Doerner *et al.* 1994; Heng *et al.* 1994; Baker & Gollub 1996) have been employed to show that, according to appropriate parameter values, the motion of the pendulum can be either regular or chaotic.

In general the results depend strongly upon the values of the parameters: both regular and chaotic attractors can arise, but never simultaneously. A systematic study of all possible scenarios arising by varying the parameter values is certainly interesting, particularly, the transition from smooth to chaotic dynamics, but we shall not perform this here, as we are interested rather in showing the complexity of features exhibited by the system: we prefer to concentrate on some values of the parameters in order to have a general picture.

We also compute the Lyapunov exponents to show sensitivity to initial conditions, thereby corroborating the fact that the system does possess the chaotic dynamics described above for suitable parameter values.

2. A forced planar pendulum

A simple pendulum of mass m and length ℓ is constrained to move in a vertical plane under the influence of gravity of intensity g, while its pivot is subjected to a vertical oscillation $y_0(t) = b\cos\omega t$, with positive b and ω; a schematic is shown in figure 1.

The governing equation of the system is given by

$$\ddot{\theta} + (\alpha - \beta\cos\tau)\sin\theta = 0, \qquad \tau = \omega t, \qquad \alpha = \frac{g}{\ell\omega^2}, \qquad \beta = \frac{b}{\ell}, \tag{2.1}$$

and the dots denote differentiation with respect to τ. This equation is referred to as the *vertically driven pendulum* equation. Its generalized dimensionless form has the advantages that

(i) of the original four parameters (g, ℓ, b, ω) only two (α, β) are left;

(ii) due to the dimensionless character of all the terms, it can be used to compare directly the dynamics of nonlinear, driven oscillators in any field, for example in mechanics, electrodynamics or solid-state physics.

Since the system is 2π periodic in θ, the fixed points are $(0, 0)$ and $(\pi, 0)$. The $(0, 0)$ fixed point corresponds to the downward state of the pendulum, while the $(\pi, 0)$ corresponds to the upward state. Equation (2.1) can not be solved analytically, but if we assume that θ remains near the equilibrium point throughout the motion, it may be linearized: linearization around $(0, 0)$ leads to

$$\ddot{\theta} + (\alpha - \beta\cos\tau)\theta = 0, \qquad \alpha = \frac{g}{\ell\omega^2}, \qquad \beta = \frac{b}{\ell}, \tag{2.2}$$

while linearization around $(\pi, 0)$, by letting $\xi = \pi + \theta$, leads to

$$\ddot{\xi} + (\alpha + \beta\cos\tau)\xi = 0, \qquad \alpha = -\frac{g}{\ell\omega^2}, \qquad \beta = \frac{b}{\ell}, \tag{2.3}$$

where now we naturally take α to be negative (in order to use the same stability diagram for both equations (2.2) and (2.3)); equations (2.2) and (2.3) are called *Mathieu's equations*. Notice that changing the sign of β amounts to shifting time by π, and therefore the invariant curves do not depend upon the sign of the parameter β. Figure 2 shows that the solutions of Mathieu's equations, depending on the values of the parameters α and β, are either stable or unstable.

Let us consider explicitly some values of the parameters. If $\alpha = 0.5$ and $\beta = 0.1$, the downward state is stable, while if $\alpha = 0.25$ and $\beta = 0.1$, it is unstable; numerically we found that this carries over to the full system (2.1), as shown in figure 3. Taking equation (2.3), if $\alpha = -0.1$ and $\beta = 0.545$, we are inside the stability region of the upward state of the pendulum, while if $\alpha = -0.2$ and $\beta = 0.1$, the upward state becomes unstable and the trajectories move away from the fixed point; again we checked numerically that this carries over to the full system, as illustrated in figure 4.

The presence of friction, unavoidable in any physical context, leads us to introduce a damping term into the equation of motion (2.1), which becomes

$$\ddot{\theta} + (\alpha - \beta\cos\tau)\sin\theta + \gamma\dot{\theta} = 0, \tag{2.4}$$

with $\gamma > 0$ denoting the *dissipative coefficient*.

The linearization of (2.4) around the two equilibrium points leads to the same equations (2.2) and (2.3) for the variables $\theta'(t) = \mathrm{e}^{\gamma t/2}\theta(t)$ and $\xi'(t) = \mathrm{e}^{\gamma t/2}\xi(t)$, respectively, provided that α is replaced with $\alpha' = \alpha - \gamma^2/4$ in both cases (see

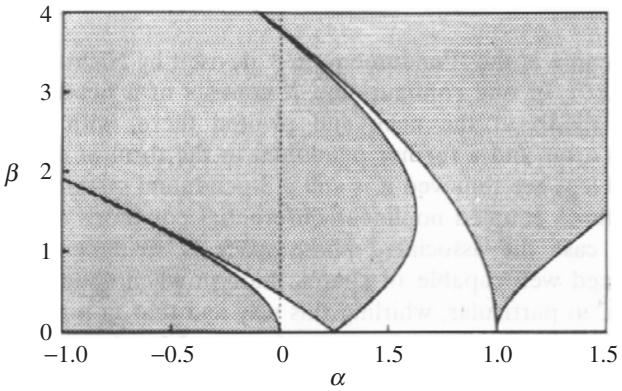

Figure 2. Stability diagram for Mathieu's equations (2.2) and (2.3). To the right of the dotted line ($\alpha = 0$), the $\theta = 0$ state is unstable in the shaded region, on the left the $\theta = \pi$ state is unstable in the shaded region. Only the region $\beta \geqslant 0$ is explicitly represented, as the diagram is even in β.

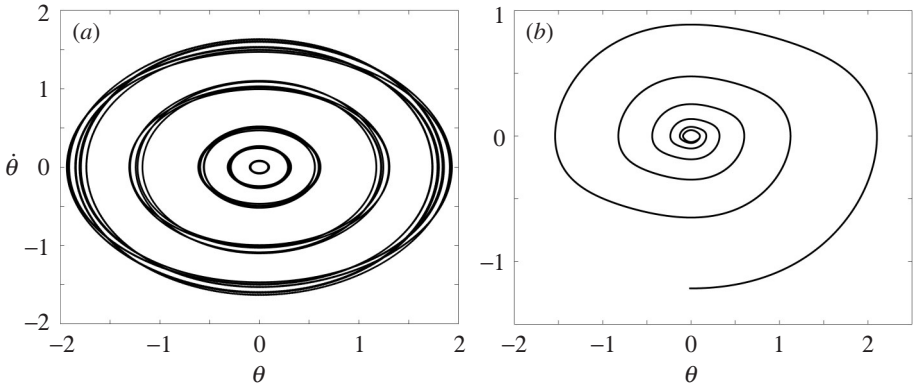

Figure 3. Stability and instability of the downward state of the pendulum described by (2.1). (*a*) Stable solutions of (2.1) when the linearized system is described by (2.2) with $\alpha = 0.5$ and $\beta = 0.1$. (*b*) An unstable solution of (2.1) when the linearized system is described by (2.2) with $\alpha = 0.25$ and $\beta = 0.1$.

Jordan & Smith 1977, ch. 8). Therefore, if γ is small enough (for practical purposes one can take γ as done below), for the values of α and β given above the behaviour of the linearized equations in presence of friction (for θ' and ξ') is the same of that of Mathieu's equations (for θ and ξ) obtained for $\gamma = 0$; it is important to note, however, that a stable equilibrium point for the linearized motion of θ' and ξ' becomes asymptotically stable for the linearized motion of the original variables θ and ξ. The stability chart of Mathieu's equation with damping,

$$\ddot{\theta} + (\alpha - \beta\cos\tau)\theta + \gamma\dot{\theta} = 0, \tag{2.5}$$

was numerically determined by Leiber & Risken (1988); to compare (2.4) with eqn (4) of Leiber & Risken (1988), we use the fact that their parameters δ and ε are related to α and β through the relations $\delta = 4\alpha$ and $\varepsilon = 2\beta$.

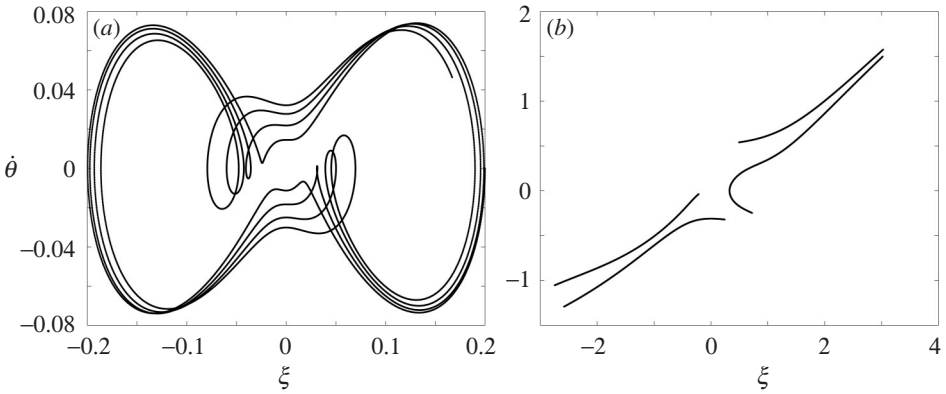

Figure 4. Stability and instability of the upward state of the pendulum described by (2.1). (*a*) Stable solution of (2.1) when the linearized system is described by (2.3) with using $\alpha = -0.1$ and $\beta = 0.545$. (*b*) Unstable solutions of (2.1) when the linearized system is described by (2.3) with $\alpha = -0.2$ and $\beta = 0.1$.

3. Attractors and basins of attraction

Given an attractor, the most direct way of determining a basin of attraction is to numerically integrate the differential equation (2.4) for each possible initial point and record those initial conditions which eventually asymptote to the attractor (see also Blackburn *et al*. 1992*b*, 1995). This approach has been used to generate high resolution basins containing as many as 1 048 576 (1024×1024 grid) initial conditions.

To characterize the attractors one can use a *phase portrait* in which the time variable is ignored, by projecting all trajectories either on the plane $(\theta, \dot\theta)$ when the downward position is stable or on the plane $(\xi, \dot\theta)$, with $\xi = \pi + \theta$, when the upward position is stable; this can be accomplished by using a DSTOOL package (see Myers *et al*. 1991).

Suppose for the sake of argument that we are studying a case in which the downward position is stable, so that we project the trajectory on the plane $(\theta, \dot\theta)$.

Note that by projecting the motion some information could be lost as to the motion of the full system: for instance a trajectory which when projected gives a closed curve can have in principle any period or could even be quasi-periodic in the space $(\theta, \dot\theta, \tau)$. We could also use Poincaré sections (as we shall do in the next section), by sampling the motion at fixed times: in this way, for instance, a periodic trajectory for the full system (including the time) should appear as a set of points in the plane $(\theta, \dot\theta)$. Nevertheless, we prefer here to project the motion on the plane $(\theta, \dot\theta)$, as this can be easier if we are only interested in revealing the smooth character of the dynamics.

Once an attractor has been found, to determine its basin of attraction we can proceed as follows. First, a small target area around the attractor was specified in the plane $(\theta, \dot\theta)$; for instance, if the attractor is the fixed point itself we can take a small rectangle of dimension 0.20×0.20 around the origin, while if the attractor is a closed curve we can take a thin strip of diameter 0.20 around the curve. Points were then selected from the grid of initial conditions and for each one a fourth-order Runge–Kutta integration routine was used to numerically integrate the system over an initial transient phase; the integration time-step (time unit) was set at 0.1 (about one-sixtieth of the drive period). After this phase, which was typically 4000 time

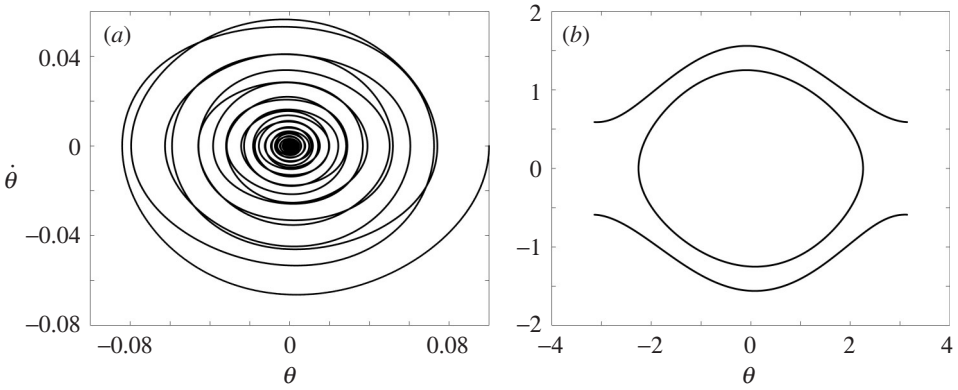

Figure 5. Attractors for the vertically driven pendulum with $\alpha = 0.5$, $\beta = 0.1$ and $\gamma = 0.03$. (*a*) A spiral orbit that goes toward the fixed point attractor. (*b*) The oscillating and the two rotating solutions.

units, a further period of integration was specified and if at any time the solution, when projected into the plane $(\theta, \dot\theta)$, entered the target area and remained there for several more time units it was assumed that that initial condition belonged to the basin of attraction for that attractor, since other attracting states were far away from the target area.

By using the above method we shall investigate the basins of attraction of our system for various values of the parameters.

(i) $\alpha = 0.5$, $\beta = 0.1$, $\gamma = 0.03$; *these values of the parameters correspond to the stability of the downward state of the linearized dynamics of the pendulum.*

(ii) $\alpha = -0.1$, $\beta = 0.545$, $\gamma = 0.08$; *these values of the parameters are in a region of stability for Mathieu's equation, and they correspond to a stable configuration for the upside-down pendulum; the dissipative coefficient is not too small because it is more difficult to stabilize the pendulum numerically in its upward state.*

(iii) $\alpha = 0.02$, $\beta = 0.35$, $\gamma = 0.03$; *for this set of values we have stability for both the upward and downward position of the linearized dynamics of the pendulum.*

Note that the dissipative coefficient should not be too small in order to stabilize the equilibrium positions numerically; on the other hand it should not be too large if one wants the stability chart of the linearized system to give some information about the stability of the full system.

(*a*) *Attractors and basins of attraction for* $\alpha = 0.5$, $\beta = 0.1$ *and* $\gamma = 0.03$

In this subsection we investigate the system (2.4) for the values of the parameters $\alpha = 0.5$, $\beta = 0.1$ and $\gamma = 0.03$. We have found that there are four coexisting attractors: the stationary state $(\theta, \dot\theta) = (0, 0)$, an oscillating solution, a clockwise running solution and a counterclockwise running solution (see figure 5).

We show in figure 6*a* the basin of attraction for the stationary solution, in figure 6*b* the basin of attraction for the oscillating solution, and finally in figure 6*c* the basins of attraction for the clockwise and anticlockwise running solutions.

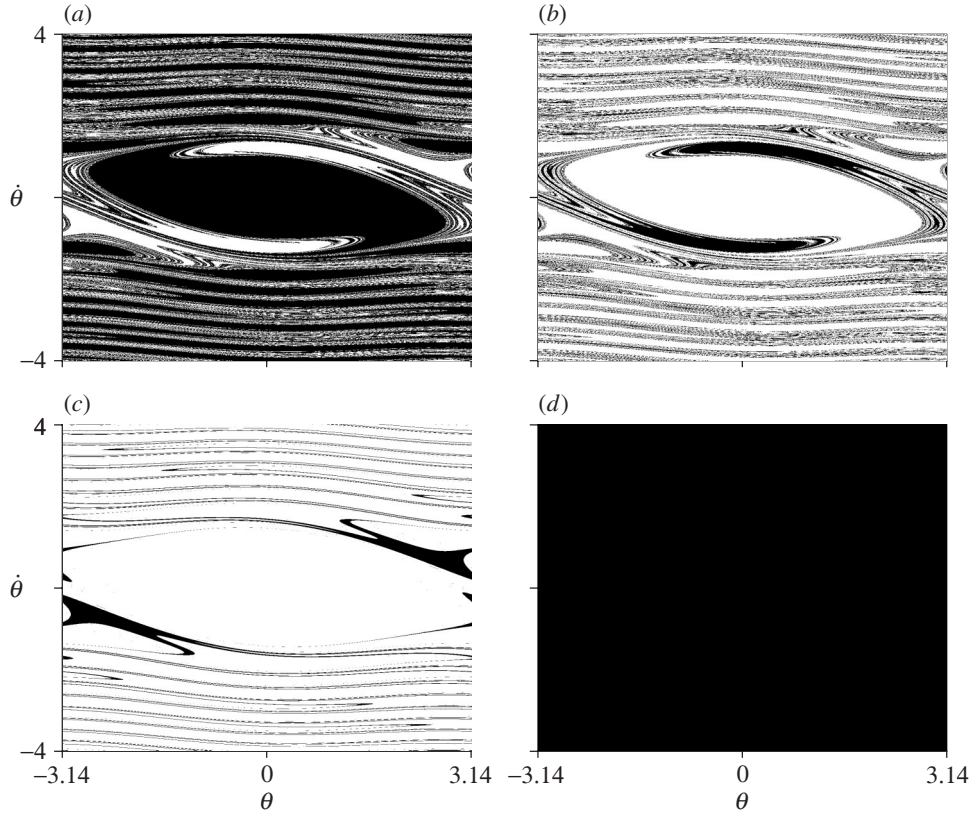

Figure 6. Coexistence of four basins of attraction (in black) for the vertically driven pendulum with $\alpha = 0.5$, $\beta = 0.1$ and $\gamma = 0.03$. (*a*) Stationary solution. (*b*) Oscillating solution. (*c*) Rotating solutions. (*d*) Union of all basins.

For initial conditions inside the black region in figure 6*a*, the trajectories converge to the fixed point $(\theta, \dot{\theta}) = (0, 0)$, as shown in figure 5*a*. For initial conditions that are inside the black region in figure 6*b*, an oscillatory behaviour can be observed after some transients: the trajectories converge to a periodic orbit, whose projection corresponds to the closed curve shown in figure 5*b*. Finally, for initial conditions that are inside the black region in figure 6*c*, a clockwise running solution and a counterclockwise running solution can be observed; due to the symmetry of the system, each of these two attractors can be found by rotating the other by π.

Figure 5 shows a phenomenon that is characteristic of nonlinear systems but cannot occur in linear systems. For the given system parameters $\alpha = 0.5$, $\beta = 0.1$ and $\gamma = 0.03$, there is a coexistence of four different attractors: depending on the initial conditions, trajectories converge towards one of these attractors (while for linear systems differences in initial conditions are damped out resulting in a single attractor).

There is strong numerical evidence that these four coexisting attractors are the only attractors for the fixed parameter values: any trajectory will ultimately end up at one of the attractors, as shown numerically in figure 6*d*, where the union of the four basins is represented.

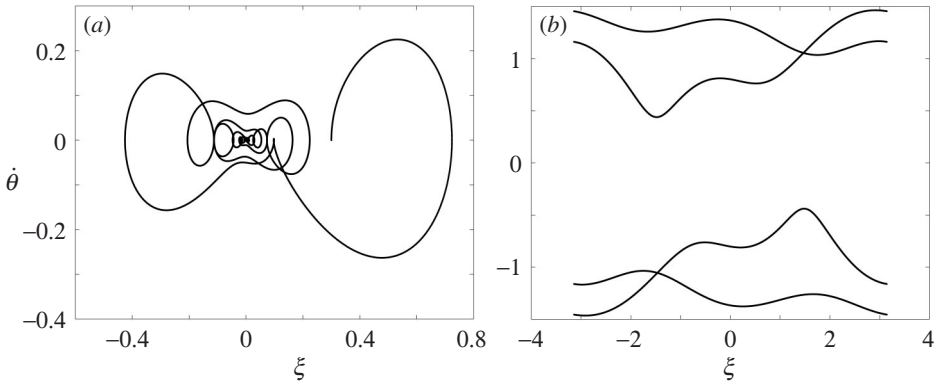

Figure 7. Attractors for the vertically driven pendulum with $\alpha = -0.1$, $\beta = 0.545$ and $\gamma = 0.08$. (a) A spiral orbit that goes toward the fixed point attractor. (b) Rotating clockwise and counterclockwise solutions.

Note that the model is invariant under the symmetry $(\theta, \dot\theta, \tau) \to (-\theta, -\dot\theta, \tau)$, so that one expects the attractors to be symmetric under inversion with respect to the origin, and in fact this is what happens. On the contrary the model is not invariant under the symmetry $(\theta, \dot\theta, \tau) \to (-\theta, \dot\theta, -\tau)$: in particular, this means that the phase portrait representation of the attractors given in figure 5b is not symmetric under reflection with respect to the axis $\theta = 0$ (as one can check by looking very carefully at the plots and by computing with accuracy the coordinates of the points of the curves). The apparent symmetry is due to the small value of γ: for $\gamma = 0$, i.e. in absence of friction, the symmetry $(\theta, \dot\theta, \tau) \to (-\theta, \dot\theta, -\tau)$ is restored and any invariant curve must be even in θ. The same symmetry considerations apply to all following plots.

(b) *Attractors and basins of attraction for* $\alpha = -0.1$, $\beta = 0.545$ *and* $\gamma = 0.08$

Consider the system (2.4) with $\alpha = -0.1$, $\beta = 0.545$ and $\gamma = 0.08$. For this case we have found that there are three coexisting attractors: the stationary state $(\theta, \dot\theta) = (\pi, 0)$, which corresponds to the upward position of the pendulum, and two other attractors which correspond to rotating (running) solutions; see figure 7b.

We show in figure 8a the basin of attraction for the stationary solution, and in figure 8b the basin for the clockwise and anticlockwise running solutions. Note that for each basin there are regions in which the structure seems to be fractal (see Smith & Blackburn 1992); for instance, figure 8a reveals a dense core surrounded by fractal layers.

Any initial condition inside the black regions in figure 8 will ultimately arrive at the corresponding attractor: for initial conditions inside the black region in figure 8a, the trajectories converge to the fixed point attractor $(\theta, \dot\theta) = (\pi, 0)$, as shown in figure 7$a$, while for initial conditions that are inside the black region in figure 8b, a clockwise running solution and an anticlockwise running solution can be observed asymptotically as shown in figure 7b. Also in this case we found that these three attractors are the only attractors (the same picture as in figure 6d is obtained by drawing simultaneously all the basins represented in figure 8).

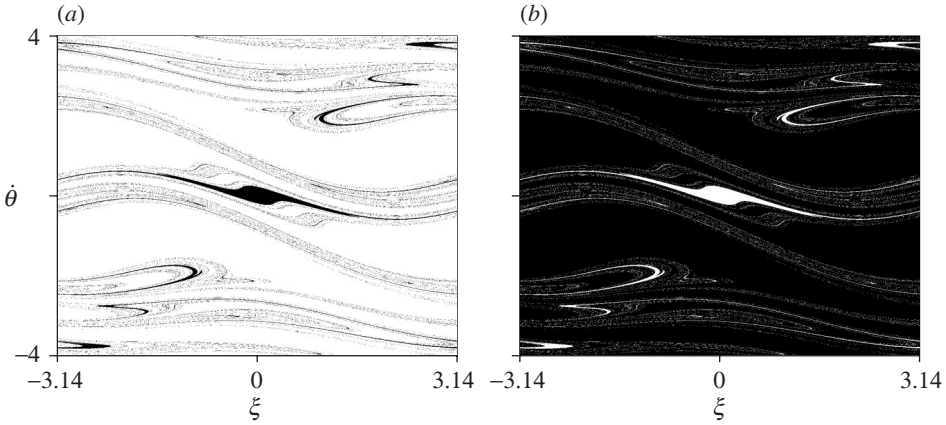

Figure 8. Coexistence of three basins of attraction (in black) for the vertically driven pendulum with $\alpha = -0.1$, $\beta = 0.545$ and $\gamma = 0.08$; one has $\xi = \pi + \theta$. (*a*) Stationary solution. (*b*) Rotating solutions.

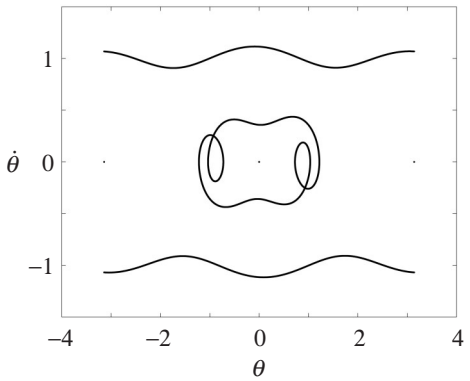

Figure 9. Attractors for the vertically driven pendulum with $\alpha = 0.02$, $\beta = 0.35$ and $\gamma = 0.03$.

(*c*) *Attractors and basins of attraction for* $\alpha = 0.02$, $\beta = 0.35$ *and* $\gamma = 0.03$

For the parameter values $\alpha = 0.02$, $\beta = 0.35$ and $\gamma = 0.03$, the downward state and the upward state are both stable; in such a case we found that there are five coexisting attractors: the two stationary states $(0, 0)$ and $(\pi, 0)$ (if we use the coordinate θ), an oscillating solution, a clockwise running solution and a counterclockwise running solution; see figure 9. The corresponding basins of attractions are given in figure 10; again their union gives the entire phase space.

The values of the parameters α and β considered so far are all inside the stability region in figure 2 (which describes the linear undamped system). What happens, as a general empirical rule, is that, if an equilibrium position is stable for Mathieu's equations (2.2) or (2.3), then it remains stable *also for the nonlinear damped equation* (2.4); this holds only approximately for the upward position of the pendulum, which would correspond to having a negative value for the parameter α; we refer to Leiber & Risken (1988) for a detailed description of the stability diagram in the linear regime. In the cases considered so far one typically finds coexistence of several smooth attractors, as in the cases explicitly worked out above. The dynamics drastically

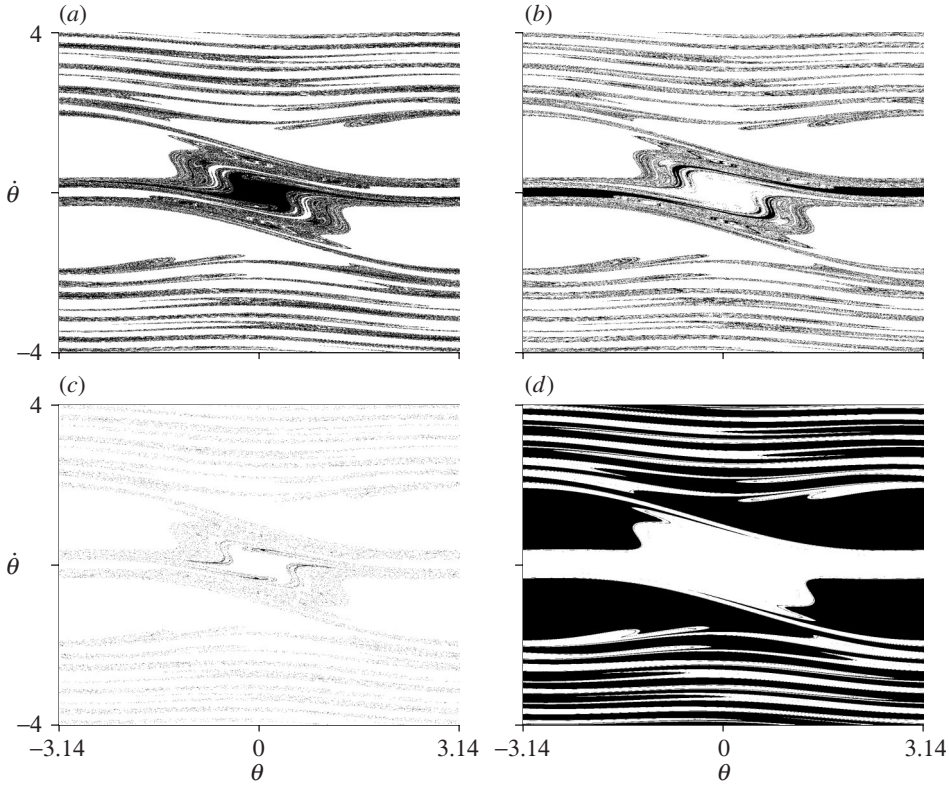

Figure 10. Coexistence of five basins of attraction (in black) for the vertically driven pendulum with $\alpha = 0.02$, $\beta = 0.35$ and $\gamma = 0.03$. (*a*) Stationary downward solution. (*b*) Stationary upward solution. (*c*) Oscillating solution. (*d*) Running solutions.

changes when one takes values of the parameters for which the fixed-point attractors are both unstable: in such cases new chaotic attractors may appear, a phenomenon which is well known in the literature (see Grebogi *et al*. 1986; Blackburn *et al*. 1992*b*). We shall discuss it in the next section.

4. Poincaré sections and strange attractors

In this section we analyse the dynamics of our system by fixing α (and γ, so that, for the linearized equation obtained from (2.4) one has a fixed value $\alpha' = \alpha - \gamma^2/4$; see § 2) and by scanning values of β along a vertical line in the plane (α, β).

We have computed the *Poincaré sections* (see Koch *et al*. 1983; Koch & Leven 1985; Leven *et al*. 1985; Michaelis 1985) obtained by removing one of the phase space dimensions (in our case the time 'τ'). The key point is that this simplified geometry nevertheless contains the essential information about the possible chaoticity of the system's dynamics. Since our system has a natural period associated with it, i.e. the period of the forcing term, the plane of the Poincaré sections could be a surface corresponding to a definite but arbitrarily chosen phase of that forcing (so in our case Poincaré sections and stroboscopic phase representations can be identified (see Eckmann & Ruelle 1985)). The choice of the plane is not crucial as long as the tra-

jectories cut the surface transversally, that is, the trajectories do not run parallel or almost parallel to the surface as they pass through. In our case the Poincaré sections are formed by recording the values of the angle and the corresponding angular velocity whenever the phase of the periodic force reaches some definite value. The pictures below qualitatively do not change if the sampling phase shift is fixed to other values, with respect to the ones explicitly considered in the figures.

(*a*) *Poincaré sections and strange attractors for* $\alpha = 0.5$ *and* $\gamma = 0.03$

For α we choose here the value $\alpha = 0.5$; from the stability diagram of Mathieu's equation, in figure 2, one can see that, for the linear case with $\gamma = 0$, see (2.2), the critical value of β for the stability of the downward state is 0.6058. For the full system (2.4) with $\gamma = 0.03$, one finds numerically for the critical value $\beta_c = 0.6063$: above β_c the stationary downward state for the linear system is unstable.

A *period-doubling* transition to chaos occurs when the parameter β is increased, starting at $\beta = 0.55$. We have detected period-doubling bifurcations up to 32-period; more precisely, for $\beta < 0.55$ a period one occurs, and at $\beta = 0.55$, 0.618, 0.6352, 0.6391, 0.6401 period-doubling bifurcations occur, leading to orbits with period 2, 4, 8, 16, 32, respectively. For instance, for $\beta = 0.63$ the Poincaré sections consist of four dots, which show that the system is tending toward an orbit on which the motion is periodic with period 4; see figure 11*b*.

For β larger than a value $\beta_d = 0.640\,18$ the motion is fully chaotic. A typical picture is shown in figure 11*d*, which gives the evolution of 1600 initial conditions (disregarding the first few iterates), for $\beta = 0.70$: we think that it represents a *strange attractor* (see Eckmann & Ruelle 1985), because the flow has a positive Lyapunov exponent as we show in § 5 below. Analogous pictures have also been found numerically for similar models (see Doerner *et al*. 1994; Leven *et al*. 1985; Smith & Blackburn 1989; Blackburn *et al*. 1992*a*). By proceeding as in § 3, we found numerical evidence that such an attractor is the only attractor in that regime.

Note that, even if the strange attractor disappears below β_d, there are still initial conditions whose first iterates appear as a sequence of dots lying over the *remnant* of the strange attractor existing above β_d before being swept towards some of the attractors, according to the scenario described by Blackburn *et al*. (1992*b*) in similar systems. This is shown in figure 12.

(*b*) *Poincaré sections and strange attractors for* $\alpha = -0.1$ *and* $\gamma = 0.08$

In this subsection we obtain similar results along the scan line β for $\alpha = -0.1$ and $\gamma = 0.08$. For the linear undamped system (2.3) the critical value for stability is $\beta = 0.618$.

For values of β less than $\beta_d = 2.145$, the system has an oscillatory behaviour, and, depending on the value of β, trajectories will eventually end up at a smooth attractor; examples are shown in figure 13.

The upward state becomes unstable at $\beta_c = 0.623$: then one has a Hopf bifurcation leading to a *flutter mode* (see Blackburn *et al*. 1992*a*): for $\beta_c < \beta < \beta_e = 0.679$ the pendulum oscillates around the vertical at half the drive frequency with an amplitude which increases with $\beta - \beta_c$; see figure 14*a*. Note that the slight tilt of the projected orbits is consistent with the symmetries of the model (which only require the attractors to be invariant under inversion with respect to the origin); we think

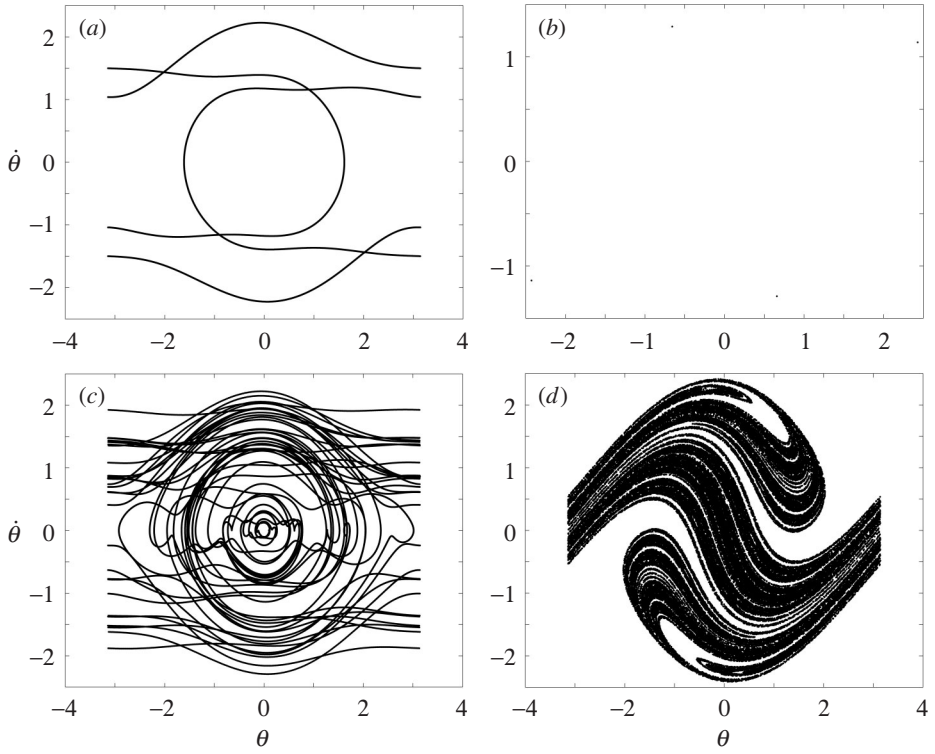

Figure 11. A chaotic trajectory and a periodic trajectory with the corresponding Poincaré sections for $\alpha = 0.5$ and $\gamma = 0.03$. The values of β are respectively $\beta = 0.70$ and $\beta = 0.63$. Transients are disregarded. (a) Periodic orbit with period 4 with initial datum $(\theta, \dot\theta) = (0.1, 0)$. ($b$) Poincaré section with sampling phase shift of 1 (in radians). (c) Chaotic trajectory with initial datum $(\theta, \dot\theta) = (0.1,0)$. ($d$) Poincaré section with sampling phase shift of 3 (in radians).

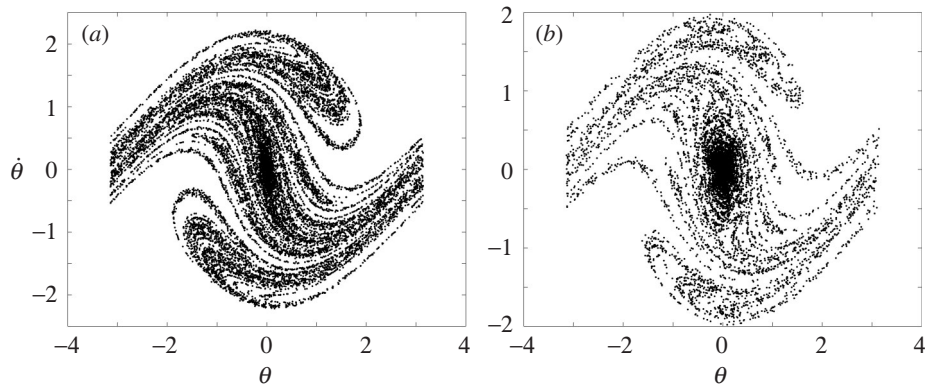

Figure 12. Strange attractor remnants for $\alpha = 0.5$ and $\gamma = 0.03$. (a) Strange attractor remnant for $\alpha = 0.5$, $\beta = 0.5$ and $\gamma = 0.03$; (b) strange attractor remnant for $\alpha = 0.5$, $\beta = 0.3$ and $\gamma = 0.03$.

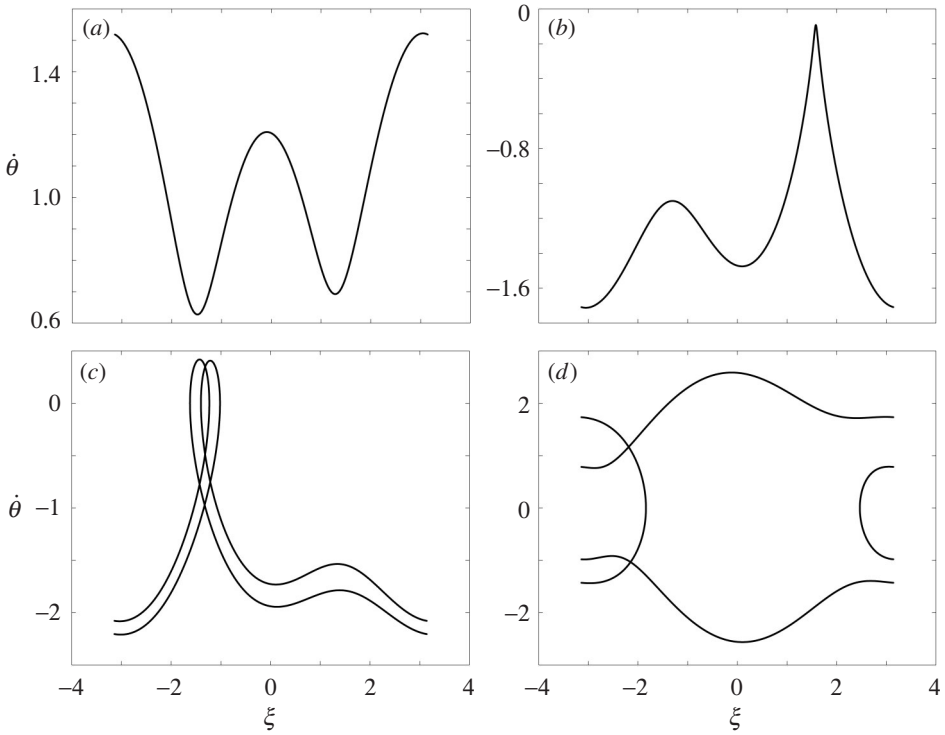

Figure 13. Smooth attractors (disregarding transients) for $\alpha = -0.1$ and $\gamma = 0.08$. (*a*) $\alpha = -0.1$, $\beta = 1.2$ and $\gamma = 0.08$. (*b*) $\alpha = -0.1$, $\beta = 1.5$ and $\gamma = 0.08$. (*c*) $\alpha = -0.1$, $\beta = 1.8$ and $\gamma = 0.08$. (*d*) $\alpha = -0.1$, $\beta = 2.1$ and $\gamma = 0.08$.

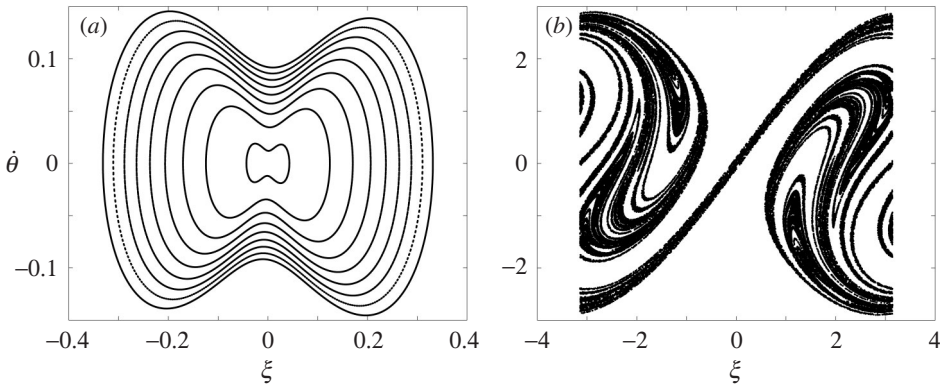

Figure 14. (*a*) Oscillating attractors corresponding to the flutter mode for $\alpha = -0.1$ and $\gamma = 0.08$, at different values of $\beta \in (0.623, 0.679)$. (*b*) Poincaré section for $\alpha = -0.1$, $\beta = 2.2$ and $\gamma = 0.08$, with sampling phase shift of 1 (in radians) of a chaotic trajectory; 1600 orbits as shown (disregarding transients).

that an equivalent tilt should also arise in the comparable plot in Blackburn *et al.* (1992*a*, *b*), and that the apparent lack of tilting in fig. 9 of the quoted paper is due to the difficulty of detecting it because of the smaller value of γ used there; see the comments at the end of § 3 *a*.

Table 1. *Computed Lyapunov exponents as β is varied; the first pair of columns corresponds to values of $\alpha = 0.5$, $\gamma = 0.03$, while the second pair corresponds to values of $\alpha = -0.1$, $\gamma = 0.08$*

β	Lyapunov exponents λ	β	Lyapunov exponents λ
0.63	−0.014 060 5	0.8	−0.039 993 8
0.64	−0.014 317 2	0.9	−0.039 980 2
0.640 18	0.010 909 3	1.3	−0.039 983
0.640 19	0.141 205	1.6	−0.039 990 5
0.65	0.179 953	1.9	−0.039 914 9
0.67	0.180 256	2.14	−0.039 559 8
0.68	0.178 863	2.145	0.024 215 3
0.69	0.179 888	2.2	0.207 936
0.70	0.179 563	2.5	0.228 123

By further increasing β the oscillating orbit disappears and only rotating attractors are left, up to the value β_{d}: again this is in agreement with the results found by Blackburn *et al.* (1992*b*) for the same model. For β taking values larger than the value of $\beta_{\mathrm{d}} = 2.145$ the motion is chaotic, as shown in figure 14*b*; this also is in accord with the value of 2.20 of the drive amplitude of Blackburn *et al.* (1995).

5. Lyapunov exponents and sensitivity to initial conditions

We found numerically that, for some parameter values, the Lyapunov exponents are positive, so that there is sensitivity to the initial conditions: this confirms the chaotic character of the motion. For a dissipative system the sum of the exponents must be negative; if the system is chaotic, then at least one of the exponents is positive. For our system there are two Lyapunov exponents corresponding to the two dimensions of the phase space $(\theta, \dot{\theta})$. In § 4, we have proposed that the Poincaré section in figures 11*b* and 14*b* represents a strange attractor. We have computed the largest Lyapunov exponent for the same parameter values we chose to obtain figures 11*b* and 14*b*. We found that for $\alpha = 0.5$, $\beta = 0.7$ and $\gamma = 0.03$ the Lyapunov exponent settles down to 0.179 563, while for $\alpha = -0.1$, $\beta = 2.2$ and $\gamma = 0.08$ the Lyapunov exponent settles down to 0.207 936. For both cases the number of time-steps was 10^7 with time unit set at 0.001. In table 1 we give a list of some computed Lyapunov exponents as β is varied. We should note here that in the chaotic regime the Lyapunov exponent is related to any initial condition that tends to the only existing attractor (i.e. figures 11*b* or 14*b*). In the non-chaotic regime, the Lyapunov exponent is related to any initial condition that tends to the corresponding among the rotating attractors found in §§ 3 and 4.

6. Concluding remarks

In this paper we investigated a planar pendulum with parametric vertical time-periodic forcing. Numerical techniques were employed to analyse the various dynamical features of the system.

First, we studied the stability of the equilibrium states (downward and upward positions) and we verified that, for initial data close to them, there is accordance

with the well-known theory of Mathieu's equation; furthermore, when such states are stable, we determined numerically their basins of attraction.

Then the existence of other attractors was investigated and their associated basins of attraction were numerically detected. Additionally, we found numerically that these were the only attractors by showing that, depending on the initial conditions, all trajectories converged towards one of them. Such results contribute towards a more complete picture of the dynamics of this system.

Finally, Poincaré sections, phase portraits and sensitivity to initial conditions provide information about the dynamics of the pendulum for specific values of the parameters α, β and γ. We found that depending on the parameter values the pendulum can show an oscillatory behaviour or an even more complicated time evolution, characterized by the existence of strange attractors. We have strengthened the latter scenario by computing the Lyapunov exponents, which turn out to be positive, as they should.

We thank Peter Ashwin and John R. Terry for use of their numerical programs for computing the basins of attractions. We also thank Philip J. Aston, Philip Kent, Sebastian Reich and John R. Terry for their help with the numerics and for useful discussions.

References

Acheson, D. J. 1993 A pendulum theorem. *Proc. R. Soc. Lond.* A **443**, 239–245.

Acheson, D. J. 1995 Multiple-nodding oscillations of a driven inverted pendulum. *Proc. R. Soc. Lond.* A **448**, 89–95.

Acheson, D. 1997 *From calculus to chaos.* Oxford University Press.

Acheson, D. J. & Mullin, T. 1993 Upside-down pendulums. *Nature* **366**, 215–216.

Baker, B. L. & Gollub, J. P. 1996 *Chaotic dynamics: an introduction.* Cambridge University Press.

Bartuccelli, M. V., Gentile, G. & Georgiou, K. V. 2001*a* KAM theorem and stability of the upside-down pendulum. Preprint. (Submitted.)

Bartuccelli, M. V., Gentile, G. & Georgiou, K. V. 2001*b* On the stability of the upside-down pendulum with damping. *Proc. R. Soc. Lond.* A. (In the press.)

Blackburn, J. A., Smith, H. J. T. & Grønbech-Jensen, N. 1992*a* Stability and Hopf bifurcations in an inverted pendulum. *Am. J. Phys.* **60**, 903–908.

Blackburn, J. A., Smith, H. J. T. & Edmundson, D. E. 1992*b* Transient chaos in a parametrically damped pendulum. *Phys. Rev.* A **45**, 593–599.

Blackburn, J. A., Grønbech-Jensen, N. & Smith, H. J. T. 1995 Stochastic noise and chaotic transients. *Phys. Rev. Lett.* **74**, 908–911.

Capecchi, D. & Bishop, S. R. 1994 Periodic oscillations and attracting basins for a parametrically excited pendulum. *Dynam. Stab. Syst.* **9**, 123–143.

Doerner, R., Hübinger, B., Heng, H. & Martienssen, W. 1994 Approaching nonlinear dynamics by studying the motion of a pendulum. II. Analyzing chaotic motion. *Int. J. Bifurcat. Chaos* **4**, 761–771.

Eckmann, J.-P. & Ruelle, D. 1985 Ergodic theory of chaos and strange attractors. *Rev. Mod. Phys.* **57**, 617–656.

Grebogi, C., Ott, E. & Yorke, J. A. 1986 Critical exponent of chaotic transients in nonlinear dynamical systems. *Phys. Rev. Lett.* **57**, 1284–1287.

Heng, H., Doerner, R., Hübinger, B. & Martienssen, W. 1994 Approaching nonlinear dynamics by studying the motion of a pendulum. I. Observing trajectories in state space. *Int. J. Bifurcat. Chaos* **4**, 751–760.

Henon, M. 1982 On the numerical computation of Poincaré maps. *Physica* D **5**, 412–414.

Hilborn, C. W. 1994 *Chaos and nonlinear dynamics*. Oxford University Press.

Jordan, D. W. & Smith, P. 1977 *Nonlinear ordinary differential equations*. Oxford: Clarendon.

Kalmus, H. P. 1970 The inverted pendulum. *Am. J. Phys.* **38**, 874–878.

Kapitsa, P. L. 1951 Dynamic stability of a pendulum with a vibrating point of suspension. *Zh. Eksp. Teoret. Fiz.* **21**, 588–598. (In Russian.) (Transl. *Collected papers by P. L. Kapitsa* (ed. D. ter Haar), vol. 2, pp. 714–726. London: Pergamon (1965).)

Koch, B. P. & Leven, R. W. 1985 Subharmonic and homoclinic bifurcations in a parametrically forced pendulum. *Physica* D **16**, 1–13.

Koch, B. P., Leven, R. W., Pompe, B. & Wilke, C. 1983 Experimental evidence for chaotic behaviour of a parametrically forced pendulum. *Phys. Lett.* A **96**, 219–224.

Landau, L. D. & Lifshitz, E. M. 1976 *Mechanics*, 3rd edn. Oxford: Pergamon.

Leiber, T. & Risken, H. 1988 Stability of parametrically exited dissipative systems. *Phys. Lett.* A **129**, 214–218.

Leven, R. W., Pompe, B., Wilke, C. & Koch, B. P. 1985 Experiments on periodic and chaotic motions of a parametrically forced pendulum. *Physica* D **16**, 371–384.

Michaelis, M. M. 1985 Stroboscopic study of the inverted pendulum. *Am. J. Phys.* **53**, 1079–1083.

Myers, M., Wicklin, R. & Worfolk, P. 1991 DSTOOL, a dynamical system toolkit with an interactive graphical interface. Center For Applied Mathematics, Cornell University.

Ness, D. J. 1967 Small oscillations of a stabilized, inverted pendulum. *Am. J. Phys.* **35**, 964–967.

Percival, I. & Richards, D. 1982 *Introduction to dynamics*. Cambridge University Press.

Pippard, A. B. 1987 The inverted pendulum. *Eur. J. Phys.* **8**, 203–206.

Poincaré, H. 1899 *Les méthodes nouvelles de la méchanique céleste*, vol. III. Paris: Gauthiers-Villars.

Smith, H. J. T. & Blackburn, J. A. 1989 Chaos in a parametrically damped pendulum. *Phys. Rev.* A **40**, 4708–4715.

Smith, H. J. T. & Blackburn, J. A. 1992 Experimental study of an inverted pendulum. *Am. J. Phys.* **60**, 909–911.

Stephenson, A. 1908 On a new type of dynamical stability. *Mem. Proc. Manch. Lit. Phil. Soc.* **52**, 1–10.